NANO LETTERS

pubs.acs.org/NanoLett

Letter

Reversibly Modulating the Blood–Brain Barrier by Laser Stimulation of Molecular-Targeted Nanoparticles

Xiaoqing Li,△ Vamsidhara Vemireddy,△ Qi Cai,△ Hejian Xiong, Peiyuan Kang, Xiuying Li, Monica Giannotta, Heather N. Hayenga, Edward Pan, Shashank R. Sirsi, Celine Mateo, David Kleinfeld, Chris Greene, Matthew Campbell, Elisabetta Dejana, Robert Bachoo,* and Zhenpeng Qin*

Cite This: https://doi.org/10.1021/acs.nanolett.1c02996

Read Online

ACCESS | Metrics & More | Article Recommendations | Supporting Information

ABSTRACT: The blood–brain barrier (BBB) is highly selective and acts as the interface between the central nervous system and circulation. While the BBB is critical for maintaining brain homeostasis, it represents a formidable challenge for drug delivery. Here we synthesized gold nanoparticles (AuNPs) for targeting the tight junction specifically and demonstrated that transcranial picosecond laser stimulation of these AuNPs post intravenous injection increases the BBB permeability. The BBB permeability change can be graded by laser intensity, is entirely reversible, and involves increased paracellular diffusion. BBB modulation does not lead to significant disruption in the spontaneous vasomotion or the structure of the neurovascular unit. This strategy allows the entry of immunoglobulins and viral gene therapy vectors, as well as cargo-laden liposomes. We anticipate this nanotechnology to be useful for tissue regions that are accessible to light or fiberoptic application and to open new avenues for drug screening and therapeutic interventions in the central nervous system.

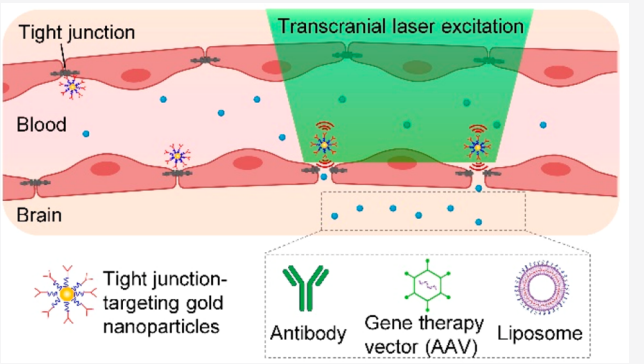

KEYWORDS: *gold nanoparticle, tight junction targeting, blood–brain barrier, therapeutics delivery*

Located at the interface between circulation and brain parenchyma, the BBB functions as a protective and regulatory interface to allow the exchange of essential nutrients while excluding the entry of the majority of hydrophilic and large molecules.[1−3] The BBB is formed by the tight-junction complex at the interfacial leaflets of brain endothelial cells (ECs) and by low levels of transcytosis through the endothelium. The BBB is dynamically regulated by pericytes and astrocytic end-feet processes and interacts with microglia and neurons to constitute the neurovascular unit.[3,4] In the development of therapeutics for CNS disorders, the BBB poses a formidable challenge for the brain delivery of systemically administered drugs. It has been estimated that the BBB excludes or limits the delivery of 98% of small-molecule and nearly all large-molecule drugs to subtherapeutic levels.[2,5] Therefore, approaches to increase the BBB permeability are essential to advance therapeutics for CNS diseases.

Biological and biophysical methods have been reported for modulating BBB permeability. These include an intrahemispheric disruption of the BBB following intracarotid artery infusion of hypertonic mannitol,[6,7] a BBB permeability increase in the whole brain by use of a vasoactive agent such as adenosine receptor agonist,[8,9] enhancing the transport across the BBB by cell-penetrating peptides and transferrin receptor targeting,[10−13] and BBB-penetrating adeno-associated virus (AAV).[14,15] More recently, focused ultrasound (FUS) excitation of circulating gas microbubbles has been shown to increase the BBB permeability in local brain regions reversibly, which is currently undergoing early-phase clinical trials with encouraging outcomes.[16,17] Currently, there are no molecularly targeted approaches for the noninvasive modulation of BBB permeability.

Due to their unique physical and chemical properties, gold nanoparticles (AuNPs) have drawn enormous interest in the biomedical field for diagnostic, imaging, and therapeutics.[18−20] We also demonstrated that the selective and remote inactivation of proteins of interest can be achieved by nanoscale-confined heating of AuNPs using nanosecond laser pulses.[21] Laser pulse excitation of AuNPs leads to several nanoscale responses, including photoacoustic heating of water

Received: August 3, 2021

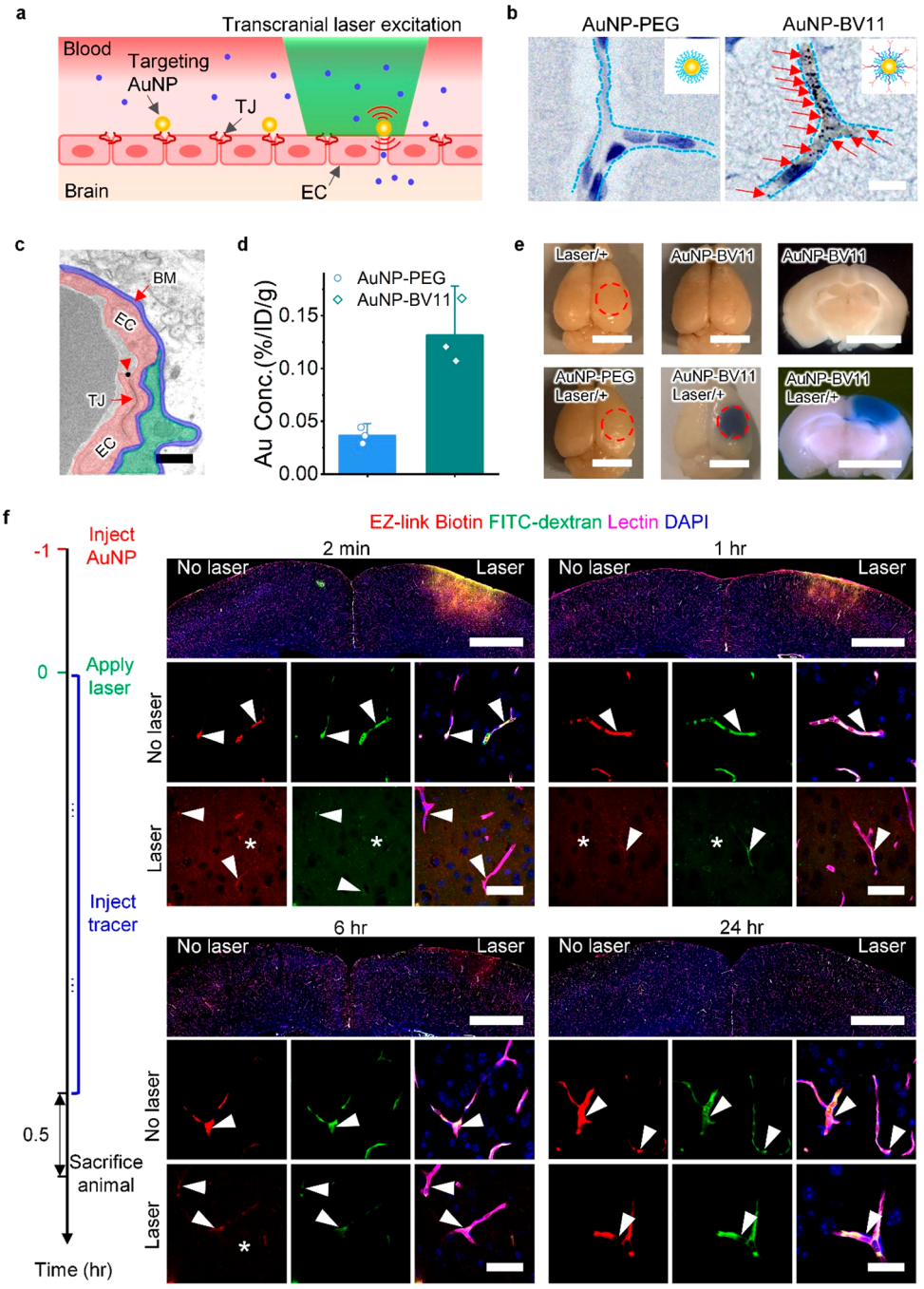

Figure 1. Picosecond stimulation of TJ-targeted nanoparticles reversibly modulates BBB permeability. (a) Schematic for transcranial laser stimulation of TJ-targeted AuNP (AuNP-BV11) for BBB modulation. Blue dots represent molecules penetrating into the brain. (b) AuNPs are visualized by silver enhancement staining in the brain. The blood vessels are outlined by dashed lines. The enhanced AuNPs are indicated by arrows. (c) AuNP-BV11 (arrowhead) colocalizes with TJ detected by EM. Pseudocolours: endothelial cell (EC, red), basement membrane (BM, blue), pericyte (P, green). (d) Quantification of AuNP-BV11 and AuNP-PEG accumulation in the brain measured by inductively coupled plasma−mass spectrometry. Each dot represents one mouse. (e) BBB modulation visualized by the leakage of albumin-binding Evans blue (25 mJ/cm^2, 1 pulse). (f) BBB permeability probed by molecular tracers (660 Da EZ-link biotin and 70 kDa fluorescein isothiocyanate (FITC) labeled dextran, 5 mJ/cm^2, 1 pulse). Blood vessels were labeled by tomato lectin-Dylight 649. The confocal images were processed with max projections of optical slices. Arrow heads indicate blood vessels, and asterisks denote dye leaked into the brain parenchyma. Scale bar: 10 μm (b), 400 nm (c), 4 mm (e), 1 mm (slide scanning images in f), 40 μm (confocal images in f). Data are expressed as mean ± SD (n = 3 mice).

molecules around the AuNPs with nanosecond laser excitation and mechanical wave generation following picosecond (ps) or femtosecond laser pulses.[22−25] Here, we present a simple nanotechnology that modulates the BBB with picosecond-laser excitation of tight junction (TJ) targeted plasmonic AuNPs. We show that the local biophysical effects generated by the interactions between AuNPs and laser pulses trigger a temporary increase in the BBB permeability, which involves diffusion through the paracellular tight junction (Figure 1a). This technology allows immunoglobulins, adeno-associated viral vectors, and liposomes to enter the brain parenchyma without inducing any discernible injury on vascular dynamics

https://doi.org/10.1021/acs.nanolett.1c02996
Nano Lett. XXXX, XXX, XXX−XXX

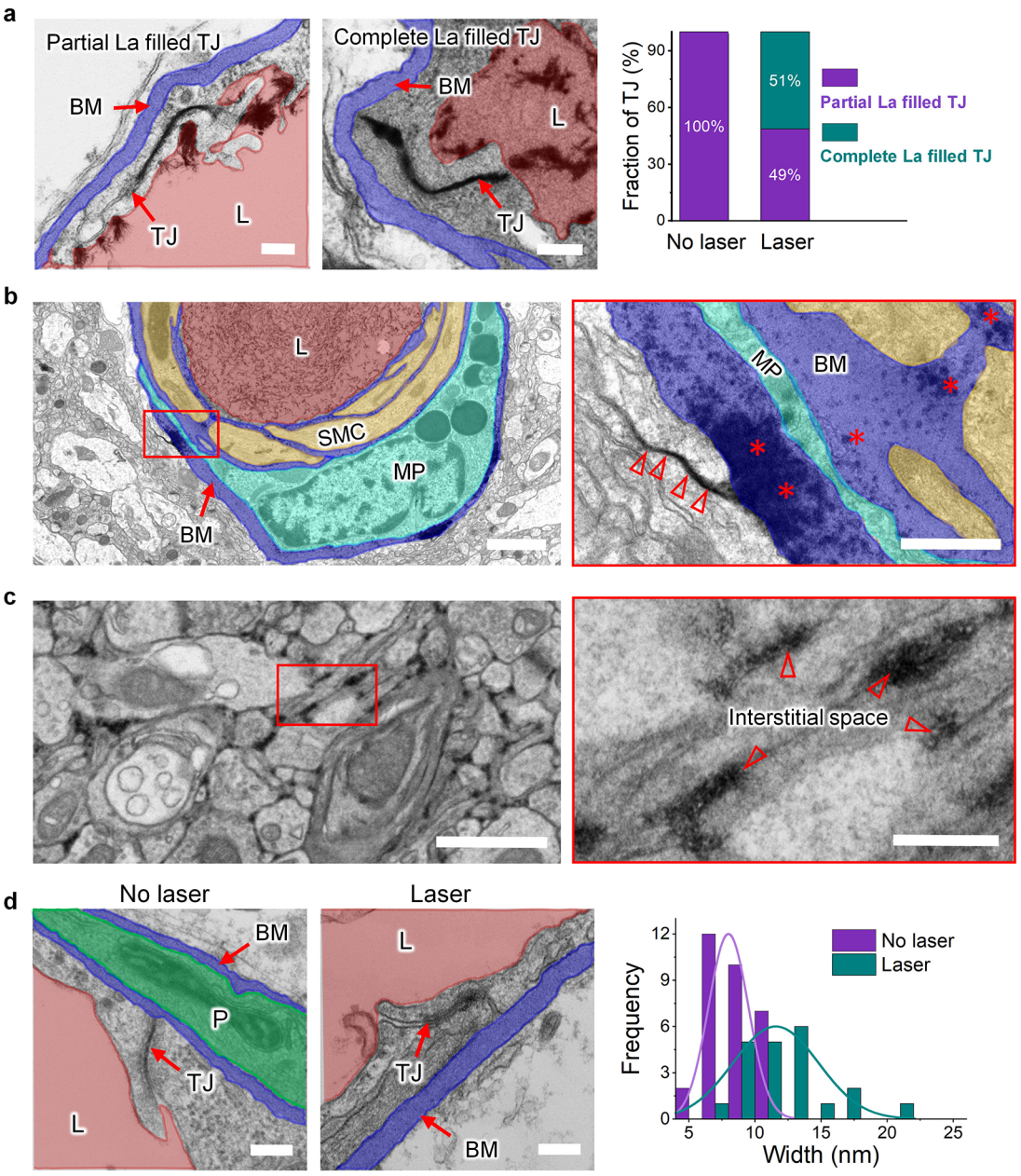

Figure 2. BBB modulation involves the paracellular route (25 mJ/cm^2, 1 pulse, 2 h post laser treatment). (a) Electron microscopy imaging of lanthanum (La)-infused TJs of brain microvasculature. Glycocalyx is visible on the lumen wall. Fifteen TJs were analyzed in the no laser group. Thirty-five TJs were analyzed in the laser group. (b) La diffusion into the basement membrane (*) and interstitial space (empty arrowheads). (c) Distribution of La in brain interstitial space (left) at the treatment region, labeled by empty arrowheads in the enlarged picture (right). (d) Electron microscopy imaging of TJs. The narrowest location of each TJ cleft was measured using Fiji/ImageJ. Thirty-one TJs were analyzed in the no laser group. Twenty-one TJs were analyzed in the laser group. Abbreviations: tight junction (TJ), lumen (L, red), basement membrane (BM, blue), pericyte (P, green), macrophage (MP, cyan). Scale bars: 200 nm ((a), (c, right), (d)), 2 μm ((b), left), 500 nm ((b), right), 1 μm ((c), left).

and brain parenchyma. These results suggest that our approach is a promising strategy to deliver therapeutic agents safely into the CNS.

RESULTS

Synthesis of TJ-Targeting AuNPs and Light Modulation of the BBB. To test the feasibility of targeting a TJ complex *in vivo*, we selected junctional adhesion molecule A (JAM-A), a single transmembrane glycoprotein that extends between the luminal surfaces of ECs and is part of the TJ complex.[26−28] Spherical 50 nm AuNPs were selected, as they have a surface plasmon resonance peak around 530 nm, which matches well with our 532 nm picosecond laser. AuNPs were then modified by antibody BV11 to specifically target JAM-A (AuNP-BV11, Figure S1). Methyl ether polyethylene glycol (mPEG) was used to backfill and stabilize AuNP-BV11. The surface of AuNPs was modified with mPEG as a nontargeting control (AuNP-PEG). We examined the biodistribution and targeting of AuNP-BV11 with intravenous (IV) injections in mice. Silver enhancement staining allows the clear visualization of AuNPs along brain vasculatures but not in the brain parenchyma in the case of AuNP-BV11, and no vasculature targeting for AuNP-PEG was observed (Figure 1b and Figure S2). Electron microscopy (EM) imaging shows that AuNP-

https://doi.org/10.1021/acs.nanolett.1c02996
Nano Lett. XXXX, XXX, XXX−XXX

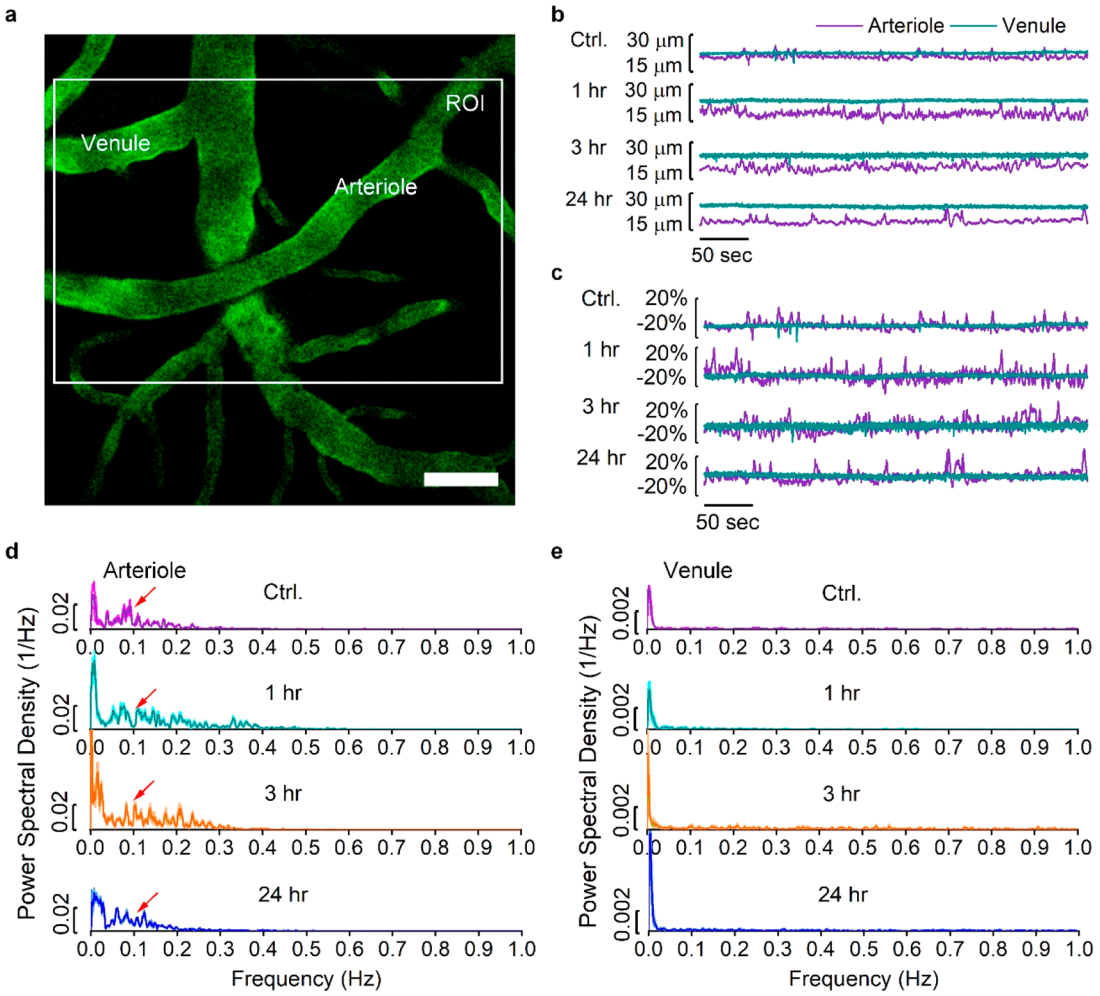

Figure 3. BBB modulation does not disrupt spontaneous vasomotion in the awake mouse (5 mJ/cm^2, 1 pulse). (a) Representative *in vivo* two-photon microscopy image of a fluorescent angiogram through a thinned-skull window in an awake, head-fixed mouse. The white box indicates a selected ROI containing a pair of an arteriole and a venule. For all of the vasomotion recordings, the arteriole and venules were imaged at 50−150 μm below the pia. (b, c) Diameter changes and percentage changes of the diameter of the arteriole and venule segment over the recorded time course. (d, e) Fourier transform analysis of the percentage change of diameter in (c), demonstrating the arteriole oscillations around 0.1 Hz ((d), indicated by the arrows). No spontaneous vasomotion in the venule segment was observed (e). Scale bar: 50 μm. Shaded areas represent SEM. Seven pairs of arterioles and venules in three mice were analyzed.

BV11 colocalizes with the TJ (Figure 1c and Figure S3). AuNP-BV11 displays 4 times higher accumulation in the brain in comparison to AuNP-PEG (Figure 1d) with the accumulation of AuNP-BV11 and AuNP-PEG in the brain at 0.13 ± 0.025%ID/g and 0.04 ± 0.006%ID/g, respectively (ID/g: injection dose per gram). AuNP-BV11 also shows a shorter circulation time (half-time of approximately 10 min for AuNP-BV11 and 2.3 h for AuNP-PEG) and organ-specific distribution (Figure S4a−e). Moreover, IV administration of AuNP-BV11 did not cause long-term systemic toxicity, as noted by the maintenance of body weight and a post-mortem histological (hematoxylin and eosin) analysis of all major organs (Figures S4f and S5). We anticipate that the AuNPs will be slowly cleared from the body through the canonical hepatobiliary pathway.[29] Estimation of the nanoparticle density suggests ∼1.5 particles/μm vessel length (Figure S6 and Table S1), or 1 AuNP seen in 200 EM images by volume (with a 10 μm by 10 μm EM image field of view and 50 nm slice thickness). Therefore, the AuNP is clearly visible on silver-stained histology but is not frequently observed in EM images. When they are taken together, these observations suggest that the systemic administration of AuNP-BV11 can selectively target the BBB along the luminal surface of vasculatures in the brain, and it has no overt toxicity.

Next, we characterized BBB permeability changes with three molecular tracers upon remote laser stimulation. We applied a 532 nm picosecond laser (1 pulse, 28 ps pulse duration, 6 mm beam diameter) transcranially to excite the TJ-targeted AuNP-BV11 at 1 h after IV injection and observed a temporary increase in BBB permeability, as indicated by Evans blue (albumin-bound, 66 kDa) leakage through the cerebral cortex and underlying corpus callosum (Figure 1e). In contrast, all control groups (laser excitation alone, AuNP-BV11 injection alone, or laser excitation following systemic administration of AuNP-PEG) failed to increase BBB permeability (Figure 1e). Moreover, the single-pulse laser excitation does not increase the tissue temperature, as detected using an infrared camera (Figure S7). We then investigated whether the duration of increased BBB permeability could be modulated by varying the laser pulse intensity. Using Evans blue as the tracer, the BBB permeability returned to the baseline at 6 h under low laser fluence (≤5 mJ/cm^2) and at 72 h with moderate and high laser

https://doi.org/10.1021/acs.nanolett.1c02996
Nano Lett. XXXX, XXX, XXX−XXX

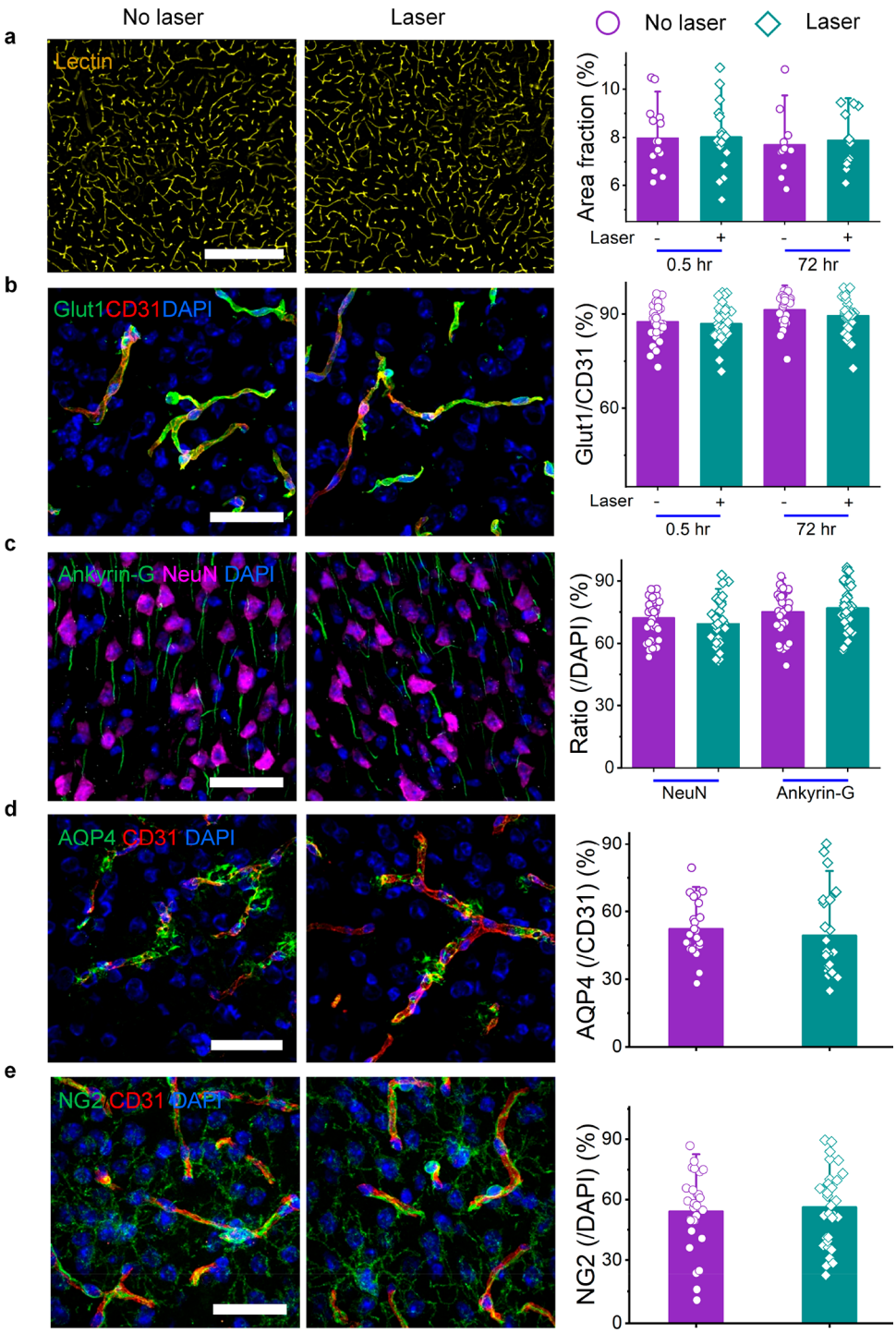

Figure 4. BBB modulation does not change the cerebral vasculature density and preserves the cellular architecture of the brain parenchyma (25 mJ/cm^2, 1 pulse). (a) Tomato lectin labeled blood vessels. Quantifying the area fraction shows no significant change in vessel density. (b) IHC staining of glucose transporters Glut1. No significant difference was measured between the normal brain and the brain after BBB modulation. (c−e) IHC staining of neuronal nucleus and axon indicated by NeuN and Ankyrin-G (c), water transporter of the astrocyte end-feet indicated by AQP4 (d), and the pericyte indicated by NG2 (e) (72 h post laser stimulation). CD31 indicates blood vessels. No significant difference was measured with and without laser treatment. Scale bar: 400 μm (a), 40 μm ((b−e)). Each dot represents a field of view (FOV). No significant difference (P > 0.05) between the "No laser" group and "Laser" group was determined using a two-sample t Test at each time point for each maker. Data are expressed as mean ± SD ($n \geq 20$ FOVs from three mice).

fluence (10−25 mJ/cm^2) (Figure S8a,b). To test if the temporal profile of increased BBB permeability was size-selective following a single laser pulse excitation (5 mJ/cm^2), we coadministered tracers of different molecular weights. Leakage of a small tracer (660 Da EZ-link biotin) was detected up to 6 h, while a large tracer (70 kDa fluorescein isothiocyanate or FITC-labeled dextran) was only detected up to 1 h after laser excitation, consistent with albumin-binding Evans blue (Figure 1f and Figure S8a−c). This size-selective pattern suggests a gradual closing of the leakage from 1 to 6 h.

https://doi.org/10.1021/acs.nanolett.1c02996
Nano Lett. XXXX, XXX, XXX−XXX

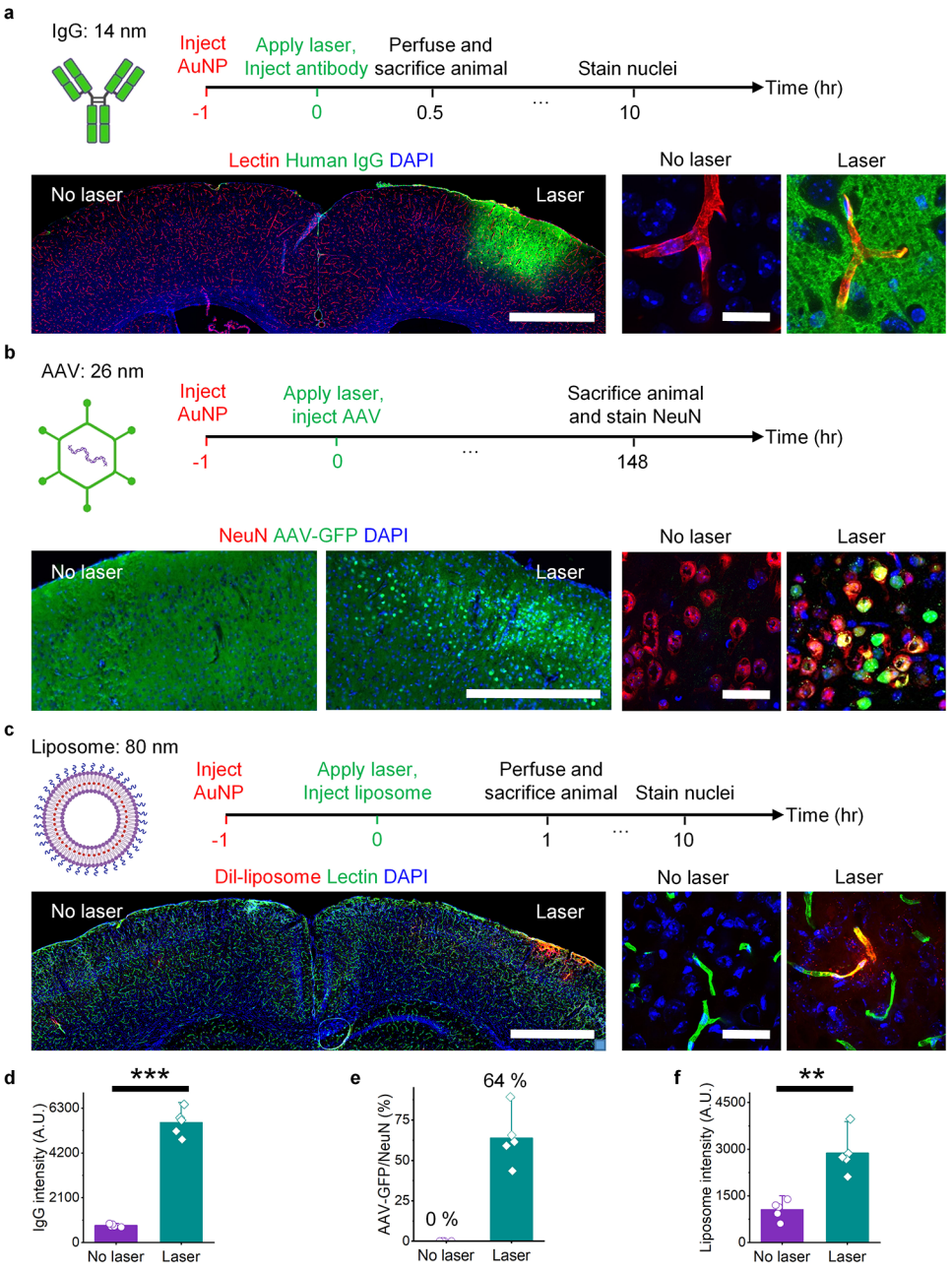

Figure 5. BBB modulation enables delivery of antibody, gene therapy vector, and liposome. (a) Delivery of human IgG antibody into the brain by BBB modulation (5 mJ/cm^2, 1 pulse). (b) Delivery of AAV-CamKII-GFP into the brain (10 mJ/cm^2, 1 pulse). (c) Delivery of liposome into the brain (5 mJ/cm^2, 1 pulse). (d–f) quantification and statistical analysis of human IgG (d), AAV-GFP (e), and Dil-liposome (f) in the ipsilateral (Laser) and contralateral hemispheres (No laser). The average intensity of each brain section (five brain sections in total) was analyzed in (a) and (c) with settings of the lower threshold level of 5005 and the upper threshold of 65535. The ratio of AAV-GFP/NeuN of confocal images in (b) was analyzed. Each dot represents a field of view (FOV). Five FOVs were analyzed. By labeling of the blood vessels with lectin, confocal images in (a) and (c) clearly show the extravasation of human IgG and Dil-liposome with laser treatment, in contrast to contralateral side without laser treatment. By staining of NeuN, the confocal image in (b) shows the colocalization of AAV-GFP and NeuN. All of the confocal images were processed with max projections of optical slices. Scale bar: 1 mm (slide scanning images in (a–c)), 40 μm (confocal images in (a–c)). Data are expressed as mean ± SD (n = 5 FOVs): **, $P < 0.01$; ***, $P < 0.001$.

No leakage of the three tracers was observed 24 h after laser excitation, suggesting that the BBB functionally recovers within this time period. Furthermore, the depth of BBB modulation (1–3 mm) is dependent on the laser fluence (2.5 to 25 mJ/cm^2), consistent with a Monte Carlo simulation of light propagation in the mouse brain (Figure S8d). The BBB modulation is restricted to the area of the laser beam with limited spillover to adjacent regions, an important feature in the targeting of sensitive and eloquent regions. Specifically, reducing the laser beam size to 2.5 and 0.8 mm allows a precise tuning of the area of BBB modulation (Figure S9a). The use of a laser fiber allows BBB modulation in deep brain regions such as the thalamus (Figure S9b).

BBB Modulation Increases the Paracellular Diffusion. To examine the routes of the BBB permeability increase (paracellular versus transcellular), we selected an electron-

https://doi.org/10.1021/acs.nanolett.1c02996
Nano Lett. XXXX, XXX, XXX−XXX

dense tracer, lanthanum nitrate, for EM detection.[29,30] We performed transcardial perfusion with 2% lanthanum nitrate (12.5 mL/min) after picosecond-laser stimulation of an AuNP-BV11 targeted brain (25 mJ/cm^2). Both ipsilateral and control cerebral cortex tissue from equivalent brain regions were processed for EM analysis (Figure S10a,b). EM images reveal that in the BBB modulation area, 51% of the TJ clefts displayed complete lanthanum (La) filling, while 49% showed partial filling (defined as the proximal portion adjacent to the lumen; Figure 2a). In contrast, in control tissue (with AuNP-BV11 infusion but no picosecond-laser stimulation) nearly 100% of the TJ clefts showed only partial filling of La (Figure 2a). Most strikingly, following laser stimulation, La was seen to diffuse beyond the TJ cleft and line the basement membrane and go into the brain interstitial space (Figure 2b,c and Figure S11). An analysis of TJ width distribution reveals the widening of TJs (Figure 2d), with 48% of the TJ width larger than 10 nm post laser treatment, while most TJs are less than 10 nm without laser treatment.[31] While we observed extravasation of La under EM, the immunofluorescence of TJ protein Claudin-5, TJ-associated protein ZO-1, and the adherens junction protein VE-cadherin did not show significant changes (Figure S12) by immunohistochemical (IHC) staining. These results suggest that the increased BBB permeability involves the passage of luminal tracers through a widening of the TJ cleft and allows diffusion of the electron-dense tracer into the brain interstitial space.

Effect of BBB Modulation on Vascular Dynamics and Brain Parenchyma. Cerebral arterioles tightly regulate the blood flow to match the metabolic demand and the supply through vessel dilation and constriction, referred to as vasomotion.[32] Disruption of the vasomotion could compromise the oxygen and nutrient supply to local brain regions. To examine whether BBB modulation impairs vasomotion, we imaged arterioles and venules (within the treated region) at 50−150 μm below the pia surface using two-photon *in vivo* imaging in awake, head-fixed mice before and after picosecond-laser stimulation (Figure 3a−c). The imaging depth is consistent with that in the literature to observe the vasomotion.[33] Fourier transform analysis suggests that, with low laser energy (5 mJ/cm^2, 1 pulse), the arteriole vasomotion (centered around 0.1 Hz) was persistent before and after BBB modulation (from 1 to 24 h, Figure 3d and Figure S13a). As expected, venules do not show vasomotion (Figure 3e and Figure S13b). Under a higher laser energy (25 mJ/cm^2, 1 pulse), the spontaneous arteriole vasomotion was attenuated from 1 h after laser stimulation and it was recovered in 72 h (Figure S13). These results suggest that BBB modulation does not impair spontaneous vasomotion at low laser energy (5 mJ/cm^2).

Next, we analyzed the structural integrity of the vasculature and the brain parenchyma after BBB modulation. There was no significant change in the cerebral vascular density, as indicated by lectin labeling of the vasculatures and by the immunofluorescence of glucose transporter-1 (Glut1) (Figure 4a,b and Figure S14). We further examined the brain ultrastructure using EM. An increase in astrocyte end-foot processes at 0.5 and 6 h post laser stimulation (Figure S15) is expected as a result of plasma proteins leaking into the brain interstitial space. There was no change in the appearance of pre- and postsynaptic processes or the mitochondrial morphology (Figure S15), and observations of Golgi silver-stained dendritic processes were similar between laser- and non-laser-treated brain regions (Figure S16). These ultrastructural observations were supported by an immunofluorescence analysis of neurons and their axonal processes (NeuN, Ankyrin-G) (Figure 4c and Figure S17). Furthermore, mural support of the BBB by an astrocyte end-foot process (AQP4) and the pericyte (NG2) were unaffected (Figure 4d,e and Figure S17). In addition, there were no significantly increased apoptotic cells 3 days after laser treatment, as determined by TUNEL staining (Figure S18). There was, however, a significant increase in Iba1$^+$ microglia processes and astrocyte GFAP expression 3 days after laser excitation (Figure S19). These indicators of reactive gliosis are entirely consistent with and are expected as a result of plasma proteins leaking into the brain. This type of reactive gliosis is thought to play a neuroprotective role.[34−36]

Antibody, Gene, and Nanoparticle Delivery to the Brain. Finally, we examined the ability of this strategy to deliver therapeutic agents, including antibodies, AAV, and liposomes. By labeling the blood vessels with lectin, we demonstrated that the systematically injected human IgG and endogenous mouse IgG could be detected in brain parenchyma at the ipsilateral hemisphere, in contrast to the contralateral hemisphere, where no IgG was detected (Figure 5a and Figure S20a,b). The analysis shows that the average fluorescent intensity of laser-treated region is much higher than that of the non-laser region (Figure 5a,d and Figure S20a), confirming the successful delivery of IgG into the brain. While there is considerable interest in developing AAV for gene therapy, local delivery requires a direct intracranial injection.[37] We intravenously injected AAV9-CamKII-GFP following picosecond-laser stimulation of AuNP-BV11. We performed IHC staining of NeuN at 1 week after laser treatment. The analysis shows 64% of cortical NeuN$^+$ neurons with clear GFP expression in the ipsilateral hemisphere in comparison to the contralateral hemisphere, which indicated no labeling (Figure 5b,e). Although some AAV serotypes have been shown to have the capability of crossing the BBB, this is dependent on the genetic background and is widespread throughout the entire brain. Focused picosecond-laser stimulation through the intact skull or direct subcortical structures by fiber optic probes will allow the precise delivery of gene therapy vectors at specific brain regions. A liposome is a versatile platform to deliver anticancer, antifungal, and antibiotic drugs.[38] To facilitate the detection of fluorescent liposome (Dil-liposome) delivery into the brain parenchyma after BBB modulation, we labeled blood vessels with lectin and perfused the animal to remove excess liposomes from the vessels. The results show the successful delivery of Dil-liposome (Figure 5c and Figure S20c), supported by the higher fluorescent intensity of Dil-liposome in the laser-treated area in comparison to the non-laser-treated region (Figure 5f and Figure S20d,e). In comparison with IgG (14 nm) and AAV (26 nm), the accumulation of liposome in the brain was lower possibly due to its relatively larger size (80 nm). Therefore, BBB modulation allows antibody, gene, and liposome penetration into the brain and indicates significant therapeutic potential.

DISCUSSION

The BBB represents a formidable challenge for brain drug delivery, as it excludes or limits over 95% of approved and investigational drugs. To overcome the BBB, we developed a nanotechnology to modulate the BBB by picosecond-laser stimulation of TJ-targeted AuNPs which, we conjecture,

https://doi.org/10.1021/acs.nanolett.1c02996
Nano Lett. XXXX, XXX, XXX−XXX

produces nanoscale pressure to loosen the TJs. It is critically important that the strategies used to increase BBB permeability minimize the risks of additional brain injury. Vasomotion has been known as vascular smooth muscle cell initiated spontaneous constrictions and dilations in arteries and arterioles at low frequencies (centered ~0.1 Hz) and is independent of pulsatile blood flow.[32,39,40] It has been shown to be the physiological basis for the blood-oxygenation-level-dependent resting-state connectivity as measured by functional magnetic resonance imaging. Our results suggest that BBB modulation does not impair vasomotion at a low laser intensity. Further experiments are necessary to investigate the effect on the nutrient supply and subsequent injury to the vulnerable brain. Moreover, using EM imaging and IHC staining, we carefully examined the effect of the BBB modulation on the brain ultrastructure parenchyma. We demonstrated that the BBB permeability can be modulated without evidence of overt injury to the brain parenchyma at the light microscope resolution or at the ultrastructural damage on EM.

In this present study, we demonstrated that the increased BBB permeability is partially due to the paracellular diffusion through the TJs. We tracked the subcellular distribution of the La tracer following BBB disruption. We observed that the La occupied the full length of the TJ clefts as well as the surrounding basement membrane. La was also seen to infiltrate into the brain interstitial spaces. Moreover, we observed that some TJ clefts became wider after BBB modulation, which has also been reported after the use of FUS to increase BBB permeability.[41] Previous studies investigated the effect of picosecond laser-AuNP stimulation on the surrounding proteins and did not find it to be effective in denaturing the targeted protein.[42,43] It is likely that there are some reversible conformation changes of TJ proteins. However, we did not detect any immunofluorescence changs of Claudin-5, ZO-1, and VE-Cadherin using IHC staining, as it cannot distinguish changes of the protein ultrastructure or redistribution. The gene and protein expression of TJ proteins could be quantified with qPCR and Western blotting. Moreover, although we did not see an increase in endocytotic vesicles by EM imaging following BBB disruption, a more systematic evaluation could be conducted using different methods such as horseradish peroxidase to elucidate the paracellular and transcellular routes involved.[44] The precise mechanism remains to be studied to clarify how the laser excitation of TJ-targeted AuNPs leads to the BBB permeability increase. Previous studies showed protein denaturation under nanosecond-laser stimulation of AuNP.[21] However, minimal protein denaturation was detected under picosecond-laser excitation.[42,43] One hypothesis is that picosecond-laser stimulation of JAM-A-targeted AuNP leads to a transient pressure variation, known as the photoacoustic effect, which leads to a Ca^{2+} influx[45,46] and activation of a second-messenger cascade and ultimately leads to an increase in the BBB permeability.

Delivering light into deep-tissue regions is key for *in vivo* photonic approaches. We demonstrated that the depth of the BBB modulation is 1−3 mm depending on the laser fluence applied. Tissue penetration can be further improved for future preclinical work and clinical translation. Optical fiber has been studied for preclinical evaluation.[47] We showed that the BBB in the deeper brain region can be modulated using an optical fiber. On the other hand, liposomes coated with AuNPs and gold nanorods can absorb near-infrared (NIR) light from 700 to 1200 nm,[24,48] while NIR light has deeper penetration into the brain.

Importantly, we anticipate that this approach has complementary applications from BBB opening using ultrasound and microbubbles. For example, it is challenging to apply ultrasound to tissues behind complicated bone structures such as the spinal cord, while it is straightforward to apply laser fiber optics in the spinal cord with minimal invasiveness.[47,49] Other targets of interest include the tumor margin around the surgical cavity of a brain tumor, since it is surgically accessible by light.[50] Future work includes delivery of a therapeutic antibody, viral and nonviral vectors for disease treatment in these targets, investigation of the precise mechanism, and long-term brain health.

CONCLUSION

In summary, we developed a straightforward nanotechnology utilizing picosecond-laser excitation of TJ-targeted AuNPs to increase the BBB paracellular permeability. This approach allows the systemic delivery of immunoglobulins, AAV particles, and liposomes to the brain. The BBB permeability increase can be graded, is entirely reversible, and does not impair cerebral vasodynamics at low laser intensity. There is no evidence of overt neuronal injury. Utilizing the local interactions of AuNPs and light, we anticipate that this research paves the way for a novel paradigm of the versatile application of AuNPs in the biomedical field. We also anticipate this nanotechnology to open new avenues for drug screening and therapeutic interventions in the central nervous system.

ASSOCIATED CONTENT

Supporting Information

The Supporting Information is available free of charge at https://pubs.acs.org/doi/10.1021/acs.nanolett.1c02996.

Additional experimental materials and methods, including AuNP conjugation, biodistribution and toxicity detection, delivery of IgG, AAV, and liposome, light propagation simulation, IHC staining, TUNEL staining, two-photon microscopy imaging, vasomotion recording and analysis, image and statistical analysis, and additional figures, including TEM, DLS, UV−vis spectroscopy, thermal images with an infrared camera, biodistribution analysis, Evans blue extravasation and analysis, slide scanning images and analysis, confocal images, and analysis (PDF)

AUTHOR INFORMATION

Corresponding Authors

Robert Bachoo − *Department of Internal Medicine and Department of Neurology, University of Texas Southwestern Medical Center, Dallas, Texas 75390, United States; Harold C. Simmons Comprehensive Cancer Center, University of Texas Southwestern Medical Center, Dallas, Texas 75390, United States*; Email: Robert.Bachoo@UTSouthwestern.edu

Zhenpeng Qin − *Department of Mechanical Engineering, University of Texas at Dallas, Richardson, Texas 75080, United States; Department of Bioengineering and Center for Advanced Pain Studies, University of Texas at Dallas, Richardson, Texas 75080, United States; Department of Surgery, University of Texas Southwestern Medical Center,*

https://doi.org/10.1021/acs.nanolett.1c02996
Nano Lett. XXXX, XXX, XXX−XXX

Dallas, Texas 75390, United States; orcid.org/0000-0003-3406-3045; Email: Zhenpeng.Qin@utdallas.edu

Authors

Xiaoqing Li − *Department of Bioengineering, University of Texas at Dallas, Richardson, Texas 75080, United States*

Vamsidhara Vemireddy − *Department of Internal Medicine, University of Texas Southwestern Medical Center, Dallas, Texas 75390, United States; Harold C. Simmons Comprehensive Cancer Center, University of Texas Southwestern Medical Center, Dallas, Texas 75390, United States*

Qi Cai − *Department of Mechanical Engineering, University of Texas at Dallas, Richardson, Texas 75080, United States*

Hejian Xiong − *Department of Mechanical Engineering, University of Texas at Dallas, Richardson, Texas 75080, United States*

Peiyuan Kang − *Department of Mechanical Engineering, University of Texas at Dallas, Richardson, Texas 75080, United States;* orcid.org/0000-0003-1784-865X

Xiuying Li − *Department of Mechanical Engineering, University of Texas at Dallas, Richardson, Texas 75080, United States*

Monica Giannotta − *FIRC Institute of Molecular Oncology Foundation (IFOM), 20139 Milan, Italy*

Heather N. Hayenga − *Department of Bioengineering, University of Texas at Dallas, Richardson, Texas 75080, United States*

Edward Pan − *Department of Neurology, University of Texas Southwestern Medical Center, Dallas, Texas 75390, United States*

Shashank R. Sirsi − *Department of Bioengineering, University of Texas at Dallas, Richardson, Texas 75080, United States;* orcid.org/0000-0002-6390-4379

Celine Mateo − *Department of Physics, University of California San Diego, La Jolla, California 92093, United States*

David Kleinfeld − *Department of Physics, University of California San Diego, La Jolla, California 92093, United States*

Chris Greene − *Smurfit Institute of Genetics, Trinity College Dublin, Dublin 2 D02 PN40, Ireland*

Matthew Campbell − *Smurfit Institute of Genetics, Trinity College Dublin, Dublin 2 D02 PN40, Ireland*

Elisabetta Dejana − *FIRC Institute of Molecular Oncology Foundation (IFOM), 20139 Milan, Italy*

Complete contact information is available at: https://pubs.acs.org/10.1021/acs.nanolett.1c02996

Author Contributions

△X.L., V.V., and Q.C. contributed equally to this work.

Author Contributions

X.L., V.V., and Q.C. designed and performed the experiments. H.X. participated in the biodistribution study, tail vein injection, and brain tissue processing. P.K. performed the simulation. X.L. participated in initiating the research idea. M.G. and E.D. developed the anti-JAM-A antibodies for this study. H.N.H., S.R.S. and E.P. participated in discussions and provided suggestions. C.M. and D.K. developed the protocol for vasomotion study. C.G. and M.C. developed the protocol for tight junction staining and EZ-link biotin detection. R.B. and Z.Q. supervised the project. All authors provided critical feedback and helped shape the research, analysis and manuscript.

Notes

The authors declare the following competing financial interest(s): A patent has been filed based on these findings (WO 2019/241623 A1).

■ ACKNOWLEDGMENTS

The authors thank the Histo Pathology Core at University of Texas Southwestern Medical Center (UTSW) for assistance with histology staining, Dr. Bret Evers for assistance with H&E analysis, the Electron Microscopy Core of UTSW for assistance with EM sample processing, Yaning Liu and Dr. Haihang Ye for assistance with EM imaging of gold nanoparticles, Xueqi Xu for assistance with liposome synthesis, Dr. Stephanie Shiers for assistance with NeuN and Ankyrin-G staining, Dr. Susanne J. van Veluw and Dr. Steven S. Hou for providing the code of vasomotion analysis, and members of the Qin laboratory for discussions. This research was funded by Cancer Prevention and Research Institute of Texas (CPRIT) grants RP160770 and RP190278 received by Z.Q., an American Heart Association Collaborative Sciences Award (19CSLOI34770004) received by Z.Q., the National Institutes of Health grant 1S10OD021685-01A1 received by the Electron Microscopy Core of UTSW, the European Research Council (project EC-ERC-VEPC, contract 742922) received by E.D., a Fondazione CARIPLO Foundation grant (2016-0461) received by M.G., and a European Research Council (ERC: Retina-Rhythm); Science Foundation Ireland (SFI) (12/YI/B2614 and 155 11/PI/1080); The Irish Research Council (IRC); The Health Research Board of Ireland (HRB); an SFI Centres grant supported in part by a research grant from SFI under grant number 16/RC/3948 and co-funded under the European Regional Development fund by FutureNeuro industry partners received by M.C.

■ REFERENCES

(1) Abbott, N. J.; Ronnback, L.; Hansson, E. Astrocyte-endothelial interactions at the blood-brain barrier. *Nat. Rev. Neurosci.* **2006**, *7* (1), 41−53.

(2) Pandit, R.; Chen, L.; Gotz, J. The blood-brain barrier: physiology and strategies for drug delivery. *Adv. Drug Delivery Rev.* **2020**, *165*−*166*, 1−14.

(3) Sweeney, M. D.; Zhao, Z.; Montagne, A.; Nelson, A. R.; Zlokovic, B. V. Blood-brain barrier: from physiology to disease and back. *Physiol. Rev.* **2019**, *99* (1), 21−78.

(4) Obermeier, B.; Daneman, R.; Ransohoff, R. M. Development, maintenance and disruption of the blood-brain barrier. *Nat. Med.* **2013**, *19* (12), 1584−1596.

(5) Pardridge, W. M. Drug transport across the blood-brain barrier. *J. Cereb. Blood Flow Metab.* **2012**, *32* (11), 1959−1972.

(6) Doolittle, N. D.; Miner, M. E.; Hall, W. A.; Siegal, T.; Hanson, E. J.; Osztie, E.; McAllister, L. D.; Bubalo, J. S.; Kraemer, D. F.; Fortin, D.; Nixon, R.; Muldoon, L. L.; Neuwelt, E. A. Safety and efficacy of a multicenter study using intraarterial chemotherapy in conjunction with osmotic opening of the blood-brain barrier for the treatment of patients with malignant brain tumors. *Cancer* **2000**, *88* (3), 637−647.

(7) Bellavance, M. A.; Blanchette, M.; Fortin, D. Recent advances in blood-brain barrier disruption as a CNS delivery strategy. *AAPS J.* **2008**, *10* (1), 166−177.

(8) Gao, X.; Qian, J.; Zheng, S.; Changyi, Y.; Zhang, J.; Ju, S.; Zhu, J.; Li, C. Overcoming the blood-brain barrier for delivering drugs into the brain by using adenosine receptor nanoagonist. *ACS Nano* **2014**, *8* (4), 3678−3689.

https://doi.org/10.1021/acs.nanolett.1c02996
Nano Lett. XXXX, XXX, XXX−XXX

(9) Carman, A. J.; Mills, J. H.; Krenz, A.; Kim, D. G.; Bynoe, M. S. Adenosine receptor signaling modulates permeability of the blood-brain barrier. *J. Neurosci.* **2011**, *31* (37), 13272−13280.
(10) Stalmans, S.; Bracke, N.; Wynendaele, E.; Gevaert, B.; Peremans, K.; Burvenich, C.; Polis, I.; De Spiegeleer, B. Cell-penetrating peptides selectively cross the blood-brain barrier in vivo. *PLoS One* **2015**, *10* (10), No. e0139652.
(11) Kariolis, M. S.; Wells, R. C.; Getz, J. A.; Kwan, W.; Mahon, C. S.; Tong, R.; Kim, D. J.; Srivastava, A.; Bedard, C.; Henne, K. R.; Giese, T.; Assimon, V. A.; Chen, X.; Zhang, Y.; Solanoy, H.; Jenkins, K.; Sanchez, P. E.; Kane, L.; Miyamoto, T.; Chew, K. S.; Pizzo, M. E.; Liang, N.; Calvert, M. E. K.; DeVos, S. L.; Baskaran, S.; Hall, S.; Sweeney, Z. K.; Thorne, R. G.; Watts, R. J.; Dennis, M. S.; Silverman, A. P.; Zuchero, Y. J. Y. Brain delivery of therapeutic proteins using an Fc fragment blood-brain barrier transport vehicle in mice and monkeys. *Sci. Transl. Med.* **2020**, *12* (545), No. eaay1359.
(12) Gao, H. Progress and perspectives on targeting nanoparticles for brain drug delivery. *Acta Pharm. Sin. B* **2016**, *6* (4), 268−286.
(13) Ruan, S.; Zhou, Y.; Jiang, X.; Gao, H. Rethinking CRITID procedure of brain targeting drug delivery: circulation, blood brain barrier recognition, intracellular transport, diseased cell targeting, internalization, and drug release. *Adv. Sci. (Weinh)* **2021**, *8* (9), 2004025.
(14) Albright, B. H.; Storey, C. M.; Murlidharan, G.; Castellanos Rivera, R. M.; Berry, G. E.; Madigan, V. J.; Asokan, A. Mapping the structural determinants required for AAVrh. 10 transport across the blood-brain barrier. *Mol. Ther.* **2018**, *26* (2), 510−523.
(15) Terstappen, G. C.; Meyer, A. H.; Bell, R. D.; Zhang, W. Strategies for delivering therapeutics across the blood-brain barrier. *Nat. Rev. Drug Discovery* **2021**, *20* (5), 362−383.
(16) Asquier, N.; Bouchoux, G.; Canney, M.; Martin, C.; Law-Ye, B.; Leclercq, D.; Chapelon, J. Y.; Lafon, C.; Idbaih, A.; Carpentier, A. Blood-brain barrier disruption in humans using an implantable ultrasound device: quantification with MR images and correlation with local acoustic pressure. *J. Neurosurg.* **2020**, *132* (3), 875−883.
(17) Rezai, A. R.; Ranjan, M.; D'Haese, P. F.; Haut, M. W.; Carpenter, J.; Najib, U.; Mehta, R. I.; Chazen, J. L.; Zibly, Z.; Yates, J. R.; Hodder, S. L.; Kaplitt, M. Noninvasive hippocampal blood-brain barrier opening in Alzheimer's disease with focused ultrasound. *Proc. Natl. Acad. Sci. U. S. A.* **2020**, *117* (17), 9180−9182.
(18) Gao, Z.; Ye, H.; Tang, D.; Tao, J.; Habibi, S.; Minerick, A.; Tang, D.; Xia, X. Platinum-decorated gold nanoparticles with dual functionalities for ultrasensitive colorimetric in vitro diagnostics. *Nano Lett.* **2017**, *17* (9), 5572−5579.
(19) Bouche, M.; Hsu, J. C.; Dong, Y. C.; Kim, J.; Taing, K.; Cormode, D. P. Recent advances in molecular imaging with gold nanoparticles. *Bioconjugate Chem.* **2020**, *31* (2), 303−314.
(20) Zhang, D.; Wu, T.; Qin, X.; Qiao, Q.; Shang, L.; Song, Q.; Yang, C.; Zhang, Z. Intracellularly generated immunological gold nanoparticles for combinatorial photothermal therapy and immunotherapy against tumor. *Nano Lett.* **2019**, *19* (9), 6635−6646.
(21) Kang, P.; Li, X.; Liu, Y.; Shiers, S. I.; Xiong, H.; Giannotta, M.; Dejana, E.; Price, T. J.; Randrianalisoa, J.; Nielsen, S. O.; Qin, Z. Transient photoinactivation of cell membrane protein activity without genetic modification by molecular hyperthermia. *ACS Nano* **2019**, *13* (11), 12487−12499.
(22) Qin, Z.; Bischof, J. C. Thermophysical and biological responses of gold nanoparticle laser heating. *Chem. Soc. Rev.* **2012**, *41* (3), 1191−1217.
(23) Lukianova-Hleb, E. Y.; Ren, X.; Sawant, R. R.; Wu, X.; Torchilin, V. P.; Lapotko, D. O. On-demand intracellular amplification of chemoradiation with cancer-specific plasmonic nanobubbles. *Nat. Med.* **2014**, *20* (7), 778−784.
(24) Xiong, H.; Li, X.; Kang, P.; Perish, J.; Neuhaus, F.; Ploski, J. E.; Kroener, S.; Ogunyankin, M. O.; Shin, J. E.; Zasadzinski, J. A.; Wang, H.; Slesinger, P. A.; Zumbuehl, A.; Qin, Z. Near-infrared light triggered-release in deep brain regions using ultra-photosensitive nanovesicles. *Angew. Chem., Int. Ed.* **2020**, *59* (22), 8608−8615.
(25) Mantri, Y.; Jokerst, J. V. Engineering plasmonic nanoparticles for enhanced photoacoustic imaging. *ACS Nano* **2020**, *14* (8), 9408−9422.
(26) Martin-Padura, I.; Lostaglio, S.; Schneemann, M.; Williams, L.; Romano, M.; Fruscella, P.; Panzeri, C.; Stoppacciaro, A.; Ruco, L.; Villa, A.; Simmons, D.; Dejana, E. Junctional adhesion molecule, a novel member of the immunoglobulin superfamily that distributes at intercellular junctions and modulates monocyte transmigration. *J. Cell Biol.* **1998**, *142* (1), 117−127.
(27) Haseloff, R. F.; Dithmer, S.; Winkler, L.; Wolburg, H.; Blasig, I. E. Transmembrane proteins of the tight junctions at the blood-brain barrier: structural and functional aspects. *Semin. Cell Dev. Biol.* **2015**, *38*, 16−25.
(28) Bazzoni, G.; Dejana, E. Endothelial cell-to-cell junctions: molecular organization and role in vascular homeostasis. *Physiol. Rev.* **2004**, *84* (3), 869−901.
(29) Poon, W.; Zhang, Y. N.; Ouyang, B.; Kingston, B. R.; Wu, J. L. Y.; Wilhelm, S.; Chan, W. C. W. Elimination pathways of nanoparticles. *ACS Nano* **2019**, *13* (5), 5785−5798.
(30) Gurnik, S.; Devraj, K.; Macas, J.; Yamaji, M.; Starke, J.; Scholz, A.; Sommer, K.; Di Tacchio, M.; Vutukuri, R.; Beck, H.; Mittelbronn, M.; Foerch, C.; Pfeilschifter, W.; Liebner, S.; Peters, K. G.; Plate, K. H.; Reiss, Y. Angiopoietin-2-induced blood-brain barrier compromise and increased stroke size are rescued by VE-PTP-dependent restoration of Tie2 signaling. *Acta Neuropathol.* **2016**, *131* (5), 753−773.
(31) Stewart, P.; Magliocco, M.; Hayakawa, K.; Farrell, C.; Del Maestro, R.; Girvin, J.; Kaufmann, J.; Vinters, H.; Gilbert, J. A quantitative analysis of blood-brain barrier ultrastructure in the aging human. *Microvasc. Res.* **1987**, *33* (2), 270−282.
(32) Mateo, C.; Knutsen, P. M.; Tsai, P. S.; Shih, A. Y.; Kleinfeld, D. Entrainment of arteriole vasomotor fluctuations by neural activity is a basis of blood-oxygenation-level-dependent "resting-state" connectivity. *Neuron* **2017**, *96* (4), 936−948.
(33) Shih, A. Y.; Mateo, C.; Drew, P. J.; Tsai, P. S.; Kleinfeld, D. A polished and reinforced thinned-skull window for long-term imaging of the mouse brain. *J. Visualized Exp.* **2012**, *61*, 3742.
(34) Faulkner, J. R.; Herrmann, J. E.; Woo, M. J.; Tansey, K. E.; Doan, N. B.; Sofroniew, M. V. Reactive astrocytes protect tissue and preserve function after spinal cord injury. *J. Neurosci.* **2004**, *24* (9), 2143−2155.
(35) Liddelow, S. A.; Barres, B. A. Reactive astrocytes: production, function, and therapeutic potential. *Immunity* **2017**, *46* (6), 957−967.
(36) Williamson, M. R.; Fuertes, C. J. A.; Dunn, A. K.; Drew, M. R.; Jones, T. A. Reactive astrocytes facilitate vascular repair and remodeling after stroke. *Cell Rep.* **2021**, *35* (4), 109048.
(37) Dodd, G. T.; Xirouchaki, C. E.; Eramo, M.; Mitchell, C. A.; Andrews, Z. B.; Henry, B. A.; Cowley, M. A.; Tiganis, T. Intranasal targeting of hypothalamic PTP1B and TCPTP reinstates leptin and insulin sensitivity and promotes weight loss in obesity. *Cell Rep.* **2019**, *28* (11), 2905−2922.
(38) Allen, T. M.; Cullis, P. R. Liposomal drug delivery systems: from concept to clinical applications. *Adv. Drug Delivery Rev.* **2013**, *65* (1), 36−48.
(39) Van Veluw, S. J.; Hou, S. S.; Calvo-Rodriguez, M.; Arbel-Ornath, M.; Snyder, A. C.; Frosch, M. P.; Greenberg, S. M.; Bacskai, B. J. Vasomotion as a driving force for paravascular clearance in the awake mouse brain. *Neuron* **2020**, *105* (3), 549−561.
(40) Chow, B. W.; Nuñez, V.; Kaplan, L.; Granger, A. J.; Bistrong, K.; Zucker, H. L.; Kumar, P.; Sabatini, B. L.; Gu, C. Caveolae in CNS arterioles mediate neurovascular coupling. *Nature* **2020**, *579* (7797), 106−110.
(41) Sheikov, N.; McDannold, N.; Vykhodtseva, N.; Jolesz, F.; Hynynen, K. Cellular mechanisms of the blood-brain barrier opening induced by ultrasound in presence of microbubbles. *Ultrasound Med. Biol.* **2004**, *30* (7), 979−989.
(42) Sarkar, D.; Kang, P.; Nielsen, S. O.; Qin, Z. Non-arrhenius reaction-diffusion kinetics for protein inactivation over a large temperature range. *ACS Nano* **2019**, *13* (8), 8669−8679.

https://doi.org/10.1021/acs.nanolett.1c02996
Nano Lett. XXXX, XXX, XXX−XXX

(43) Huettmann, G.; Radt, B.; Serbin, J.; Birngruber, R. Inactivation of proteins by irradiation of gold nanoparticles with nano-and picosecond laser pulses. *Proc. SPIE* **2003**, *5142*, 88−95.
(44) Andreone, B. J.; Chow, B. W.; Tata, A.; Lacoste, B.; Ben-Zvi, A.; Bullock, K.; Deik, A. A.; Ginty, D. D.; Clish, C. B.; Gu, C. Blood-brain barrier permeability is regulated by lipid transport-dependent suppression of caveolae-mediated transcytosis. *Neuron* **2017**, *94* (3), 581−594.
(45) Tran, Q. K.; Ohashi, K.; Watanabe, H. Calcium signalling in endothelial cells. *Cardiovasc. Res.* **2000**, *48* (1), 13−22.
(46) Dalal, P. J.; Muller, W. A.; Sullivan, D. P. Endothelial cell calcium signaling during barrier function and inflammation. *Am. J. Pathol.* **2020**, *190* (3), 535−542.
(47) Busch, D. R.; Davis, J.; Kogler, A.; Galler, R. M.; Parthasarathy, A. B.; Yodh, A. G.; Floyd, T. F. Laser safety in fiber-optic monitoring of spinal cord hemodynamics: a preclinical evaluation. *J. Biomed. Opt.* **2018**, *23* (6), 1−9.
(48) Chen, Y. S.; Zhao, Y.; Yoon, S. J.; Gambhir, S. S.; Emelianov, S. Miniature gold nanorods for photoacoustic molecular imaging in the second near-infrared optical window. *Nat. Nanotechnol.* **2019**, *14* (5), 465−472.
(49) Zuo, X.; Liang, Z.; Zhang, J.; Wang, S.; Zheng, Q.; Ma, Y.; Li, P.; Ding, T.; Hu, X.; Wang, Z. Photobiomodulation and diffusing optical fiber on spinal cord's impact on nerve cells from normal spinal cord tissue in piglets. *Lasers Med. Sci.* **2021**.
(50) Sarkaria, J. N.; Hu, L. S.; Parney, I. F.; Pafundi, D. H.; Brinkmann, D. H.; Laack, N. N.; Giannini, C.; Burns, T. C.; Kizilbash, S. H.; Laramy, J. K.; Swanson, K. R.; Kaufmann, T. J.; Brown, P. D.; Agar, N. Y. R.; Galanis, E.; Buckner, J. C.; Elmquist, W. F. Is the blood-brain barrier really disrupted in all glioblastomas? A critical assessment of existing clinical data. *Neuro Oncol* **2018**, *20* (2), 184−191.

https://doi.org/10.1021/acs.nanolett.1c02996
Nano Lett. XXXX, XXX, XXX−XXX